ELSEVIER

Journal of Crystal Growth 166 (1996) 436–445

JOURNAL OF CRYSTAL GROWTH

Numerical simulation of convective three-dimensional flows in a horizontal cylinder under the action of a constant magnetic field

H. Ben Hadid *, D. Henry

Laboratoire de Mécanique des Fluides et d'Acoustique, UMR CNRS 5509, Ecole Centrale de Lyon / Université Claude Bernard, Lyon 1, ECL, BP 163, F-69131 Ecully Cedex, France

Abstract

The effects of a constant magnetic field on electrically conducting liquid-metal flows in a cylindrical cavity corresponding to horizontal Bridgman growth are investigated numerically by solving the Navier–Stokes and Ohm equations for three-dimensional flows. The increase in the strength of the applied magnetic field leads to several fundamental changes in the properties of the thermal buoyant convection. The convective circulation progressively loses its intensity and is reorganized specifically depending on the direction (vertical, longitudinal or transversal) of the applied magnetic field. The characteristic behaviours observed correspond to the appearance of specific velocity profiles, of Hartmann layers and of parallel layers, and to the tendency towards two dimensionality. These structural changes are in fact closely connected to the repartition of the induced electric current inside the cavity.

1. Introduction

The paper is focused on the action of a constant magnetic field on the flow that develops in a differentially heated Bridgman cylindrical cavity. For such three-dimensional buoyancy-driven flows, we investigated the effect of the orientation and intensity of a constant magnetic field. In the literature different studies can be found on buoyancy-induced flows in horizontal cylinders [1–3] and on the action of a magnetic field on convective flows (see Refs. [4–8]). To our knowledge there is no result available on the magnetic damping in horizontal three-dimensional cylindrical Bridgman configurations, except recent works performed for a vertical magnetic field, experimentally with a cylindrical cell filled with mercury and numerically by two-dimensional simulations in cross-sectional planes [9].

In this study the structural changes of the flow induced by the magnetic field are put into light for each field orientation. An attempt on understanding is then proposed by showing the connection with the induced current distribution inside the cavity.

2. Mathematical model

We consider a cylindrical cavity of diameter D and length L (Fig. 1) filled with an electrically conducting liquid metal. The aspect ratio of the cavity is chosen as $A = L/D = 4$. Owing to the temperature difference between the end walls, hori-

* Corresponding author.

PII S0022-0248(96)00044-9

zontal temperature gradients form throughout the cavity and generate a laminar convective motion.

The basic equations used in the simulations of the melt flow are the Navier–Stokes equations including the Lorentz force and using the Boussinesq approximation for buoyancy since the metallic liquid is considered incompressible. The three-dimensional conservation equations of momentum are made dimensionless using D, D^2/ν, $U_{\mathrm{ref}} = \nu/D\ \mathrm{Gr}^{1/2}$, $\Delta T/A$, $\boldsymbol{B}_0$ and $\sigma_e U_{\mathrm{ref}}|\boldsymbol{B}_0|$ as scales for length, time, velocity, temperature, magnetic flux density and electric current density respectively (ν is the kinematic viscosity, σ_e the electrical conductivity of the melt and $\Delta T = T_h - T_c$ the difference of temperature between the vertical end walls). Using these nondimensionalizations the governing equations in the melt may be written as

$$\nabla \cdot \boldsymbol{v} = 0, \tag{1}$$

$$\partial \boldsymbol{v}/\partial t + \mathrm{Gr}^{1/2}(\boldsymbol{v}\cdot\nabla)\boldsymbol{v} = -\nabla p + \nabla^2 \boldsymbol{v} + \mathrm{Gr}^{1/2}\theta \boldsymbol{e}_y + \mathrm{Ha}^2 \boldsymbol{J} \times \boldsymbol{e}_{\mathbf{B}_0}, \tag{2}$$

$$\partial\theta/\partial t + \mathrm{Gr}^{1/2}(\boldsymbol{v}\cdot\nabla)\theta = \mathrm{Pr}^{-1}\nabla^2\theta, \tag{3}$$

where $\boldsymbol{v}$ is the dimensionless velocity field ($\boldsymbol{v} = (u,v,w)$), p denotes the dimensionless static pressure, $\boldsymbol{e}_{\mathbf{B}_0}$ the unit vector in the direction of $\boldsymbol{B}_0$ and θ is the dimensionless temperature defined as $\theta = A(T - T_m)/\Delta T$, where $T_m = (T_h + T_c)/2$. In the present study we generally set the Prandtl number equal to 0.026, a value corresponding to experiments with mercury [9]. The magnetic flux density vector $\boldsymbol{B}$ in the Lorentz force is set equal to $\boldsymbol{B}_0$ (the applied field) as the induced field $\boldsymbol{b}$ is small ($\mathrm{Re}_m \ll 1$, where Re_m is the magnetic Reynolds number). The dimensionless electric current density $\boldsymbol{J}$ is given by Ohm's law for a moving fluid

$$\boldsymbol{J} = \boldsymbol{E} + \boldsymbol{v} \times \boldsymbol{e}_{\mathbf{B}_0}, \tag{4}$$

where $\boldsymbol{E}$ is the dimensionless electric field. Here, since all the melt flows studied are steady, the electric field can be written as the gradient of an electric potential ($\boldsymbol{E} = -\nabla\psi_e$). The equation of continuity for the electric current density gives

$$\nabla \cdot \boldsymbol{J} = 0, \tag{5}$$

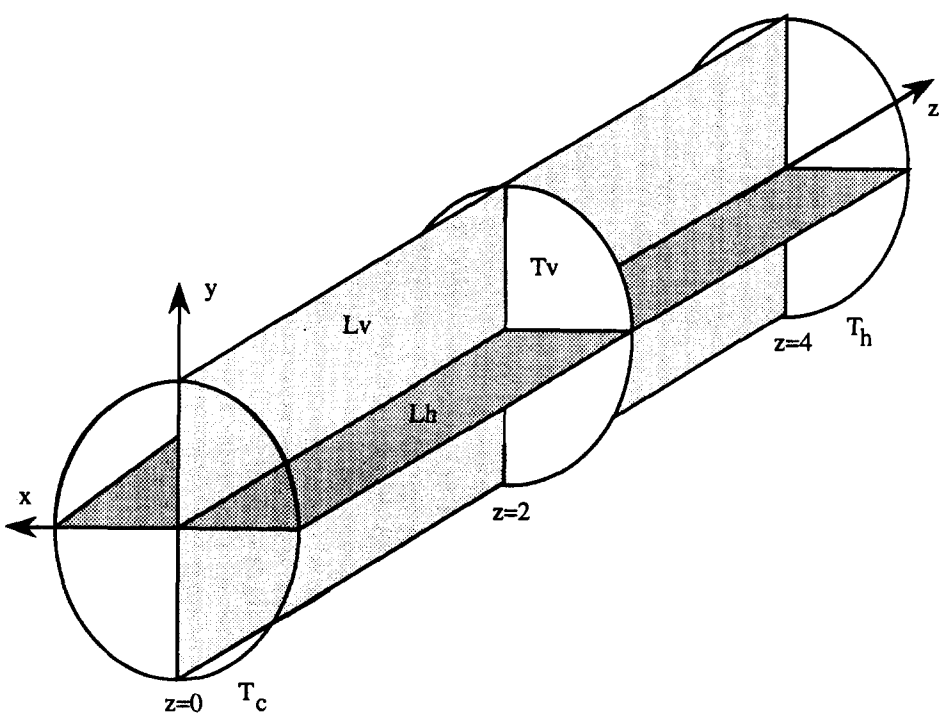

Fig. 1. Geometry of the cylindrical cavity and of the frame of reference.

which, combined with Eq. (4), leads to

$$\nabla^2 \psi_e = \nabla \cdot (\boldsymbol{v} \times \boldsymbol{e}_{\mathbf{B}_0}). \tag{6}$$

The boundary conditions for the velocity are the usual no-slip conditions $u = v = w = 0$ at any wall. The thermal boundary conditions correspond to isothermal end walls and insulated lateral walls (i.e. $\nabla T \cdot \boldsymbol{n} = 0$). For the electric current density, $\boldsymbol{J}$, insulated conditions $\boldsymbol{J} \cdot \boldsymbol{n} = 0$ are adopted at all the boundaries.

The dimensionless parameters appearing in Eqs. (2) and (3) are the Grashof number $\mathrm{Gr} = g\beta\Delta T D^4/L\nu^2$, the Prandtl number $\mathrm{Pr} = \nu/\kappa$ and the Hartmann number $\mathrm{Ha} = |\boldsymbol{B}_0|\boldsymbol{D}\ (\sigma_e/\rho\nu)^{1/2}$, where β is the coefficient of volumetric expansion and κ the thermal diffusivity.

The spatial discretization of the governing Eqs. (1)–(6) is based on an isoparametric spectral element method [10] which is a high-order weighted residual technique. The cylindrical geometry is divided in five subdomains; in each one $9 \times 9 \times 27$ (following x, y and z respectively) Gauss–Lobatto–Legendre collocation points were used. The time-discretization of Eqs. (2) and (3) employs a high-order time-differencing scheme combined with a splitting algorithm [11].

3. Numerical results

This paper focuses on the changes in the characteristics of the liquid-metal flow as the Hartmann number is increased for different orientations of the magnetic field, namely, along the x, y and z directions. The flow is first studied without magnetic field for Grashof numbers up to 1.5×10^5. Then, to study the action of the magnetic field, the Grashof number will be set equal to 5×10^4. In the following, different planes will be used inside the cavity to characterize the results (Fig. 1): the (Lv)-plane (longitudinal vertical middle plane, main plane of circulation), the (Lh)-plane (longitudinal horizontal middle plane), and the (Tv)-plane (transverse vertical middle plane).

The original symmetries in such a confined cavity are a reflexion symmetry with respect to the (Lv)-plane and a reflexion symmetry with respect to the (Th)-line (transverse horizontal centre line). The combination of these two symmetries gives also a symmetry with respect to the centre point of the

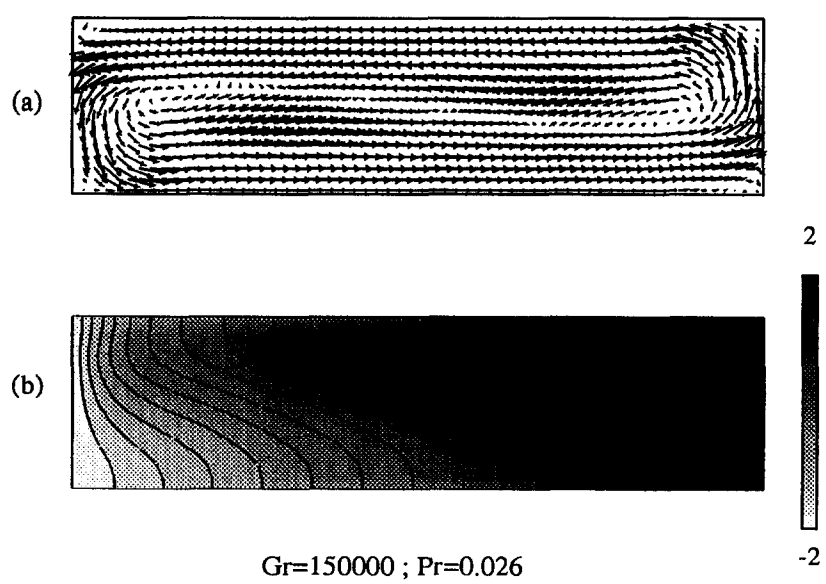

Fig. 2. Velocity vectors (a) and temperature isovalues (b) in the (Lv)-plane for $\mathrm{Gr} = 1.5 \times 10^5$, $\mathrm{Pr} = 0.026$ and $\mathrm{Ha} = 0$.

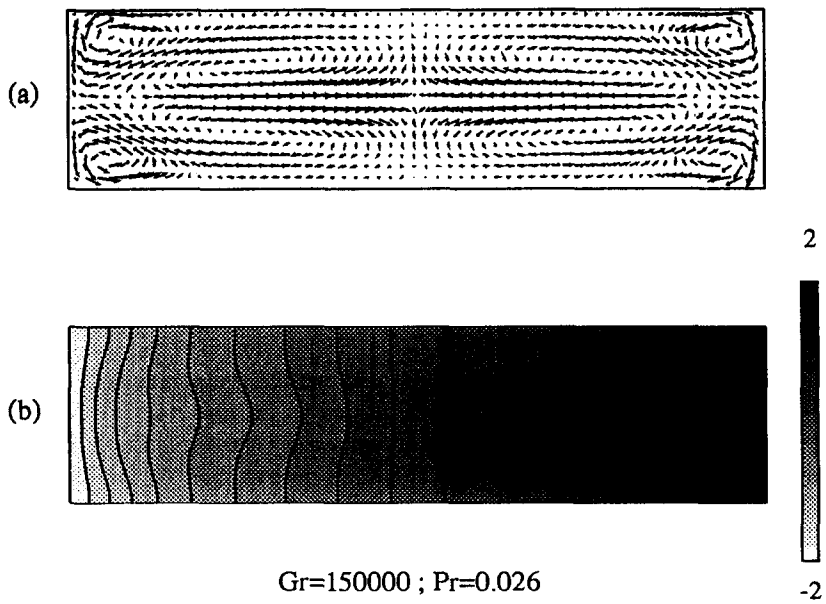

Fig. 3. Velocity vectors projection (a) and temperature isovalues (b) in the (Lh)-plane for $Gr = 1.5 \times 10^5$, $Pr = 0.026$ and $Ha = 0$.

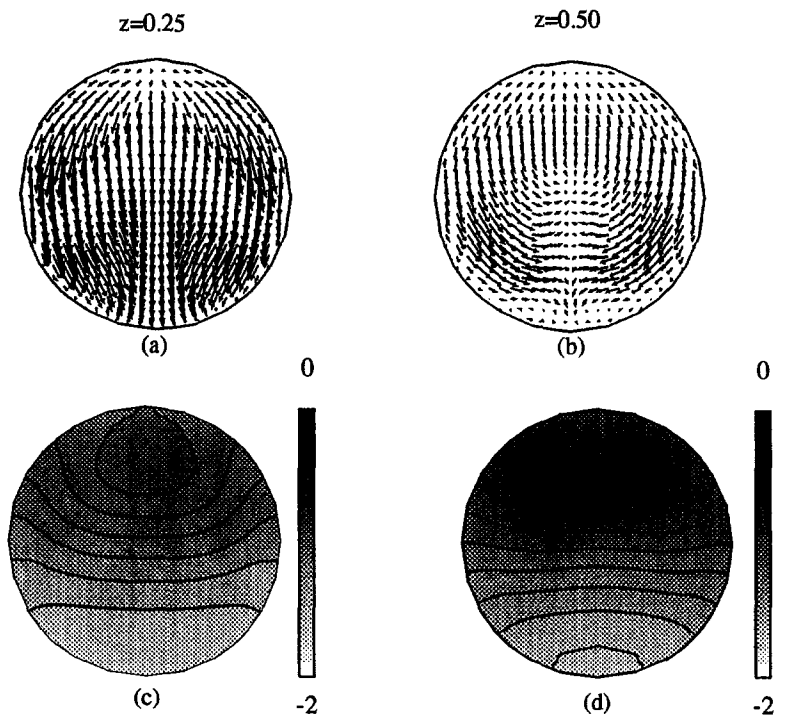

Fig. 4. Velocity vectors projection (a,b) and temperature isovalues (c,d) in cross-sectional planes at $z = 0.25$ and $z = 0.5$ for $Gr = 1.5 \times 10^5$, $Pr = 0.026$ and $Ha = 0$.

cavity. In all the cases we have studied, these symmetries are found to remain valid.

3.1. Buoyancy flow without magnetic field

For small and moderate Grashof numbers $Gr < 5 \times 10^4$, the buoyancy flow in the cylindrical cavity corresponds to two horizontal counterflows moving from the hot wall above, and from the cold wall below. When the Grashof number is further increased, up to $Gr = 1.5 \times 10^5$, the flow remains steady but progressive modifications in the flow structure are observed. In the (Lv)-plane (Fig. 2a), the main feature is the onset of secondary vortices in the end regions inside the large convective loop. These vortices, already visible for $Gr = 5 \times 10^4$, are fully developed for $Gr = 1.5 \times 10^5$, where they clearly affect the circulation in the (Lh)-plane (Fig. 3a). Small recirculations appear also in the vicinity of the bottom corner of the hot wall and at the top corner of the cold wall (Fig. 2a). Other modifications correspond to the development of the three-dimensional character of the flow, particularly in the end parts of the cavity, with motions of fluid between the zones near the (Lv)-plane and the zones closer to the circular lateral walls (Fig. 3a and Fig. 4a–4b). In order to improve the flow description given in the previous figures, the fully three-dimensional velocity vectors field at four cross-sectional planes is given in Fig. 5. The analysis of the figure confirms the three-dimensional character of the flow. Fig. 5 also reveals the strong modification of the flow structure along the longitudinal direction. The flow is rather concentrated near the (Lv)-plane when it leaves the end walls and then it is spread out over the whole width.

The temperature field is affected by the flow, but despite the large Gr numbers the deformations remain not too large because the fluid considered is a good thermal conductor ($Pr = 0.026$) (Figs. 2b, 3b and 4c–4d). In the range of Gr studied, the parallel flow regime with constant temperature gradient in the central part of the cavity is no more valid except for the smallest Gr ($Gr = 2 \times 10^4$).

The evolution of the maximum of the longitudinal and vertical velocities with the Grashof number is found to be linear up to $Gr = 2 \times 10^4$. For higher values of Gr the trend of the velocities is to increase more slowly than Gr but without reaching the expected $Gr^{1/2}$ asymptotic behaviour. This corresponds to the transition from the core-driven regime to the boundary-layer-driven regime.

3.2. Vertical magnetic field (B_y case)

When the constant magnetic field is applied vertically, an analytical horizontal velocity profile can be obtained in the core of the cavity by two-dimensional considerations [12]. This profile, which is given by

$$w = -\frac{\mathrm{Gr}}{\mathrm{Ha}^2} y, \tag{7}$$

is linear with respect to the vertical direction and its intensity decreases strongly with Ha. It is connected to the lower and upper rigid boundaries by classical Hartmann exponential profiles.

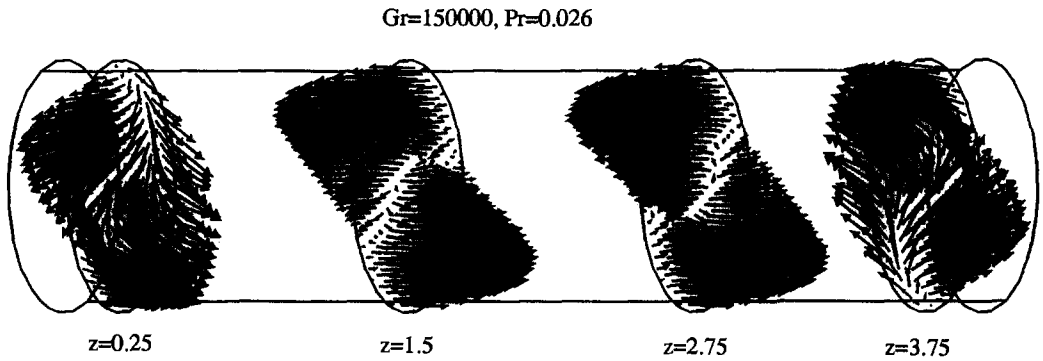

Fig. 5. Three-dimensional velocity vectors field given in four cross-sectional planes ($z = 0.25$, 1.5, 2.75, 3.75) for $Gr = 1.5 \times 10^5$, $Pr = 0.026$ and $Ha = 0$.

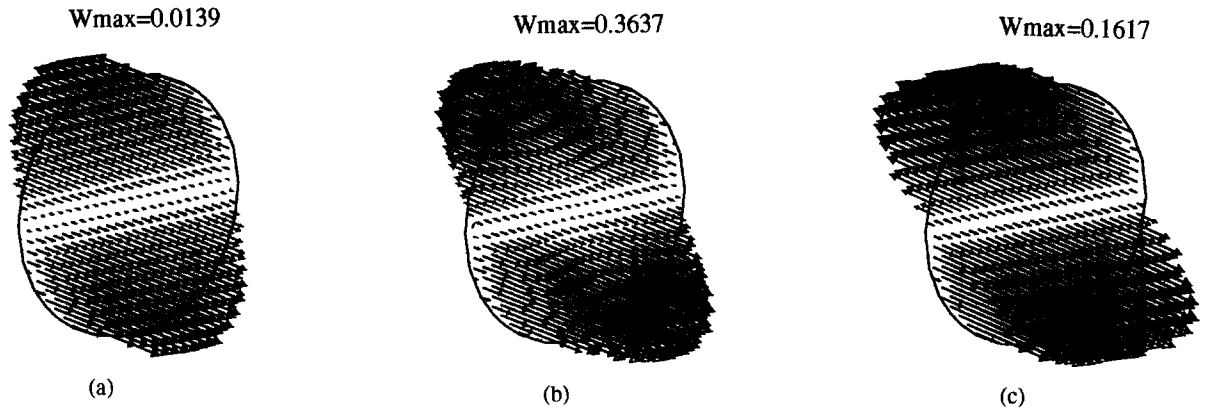

Fig. 6. Velocity vectors in the (Tv)-plane at Gr = 5×10^4 and Ha = 150 for three orientations of the applied magnetic field ((a) B_y case, (b) B_z case, and (c) B_x case).

The results obtained in cylindrical cavities present similar behaviours. As the Hartmann number is increased, the horizontal velocity profiles (Fig. 6a), originally (i.e. Ha = 0) with a S-shape, evolve to a linear profile, which becomes valid along the whole transverse direction (tendency towards two-dimensionality of the flow). The flow becomes also progressively independent of the longitudinal direction z in the central part of the cavity and almost anti-symmetric with respect to the (Lh)- and (Tv)-planes (Fig. 7a).

The flow evolution obtained in the cavity is connected to the structure of the induced electric current. As is clear from Eq. (4), the current is composed of two parts: the directly induced part ($\boldsymbol{v} \times \boldsymbol{e}_{\mathbf{B}_0}$) and the potential part created by the electric potential ($-\nabla\psi_e$). In the present case, the electric current corresponds to large circular loops in the cross-sec-

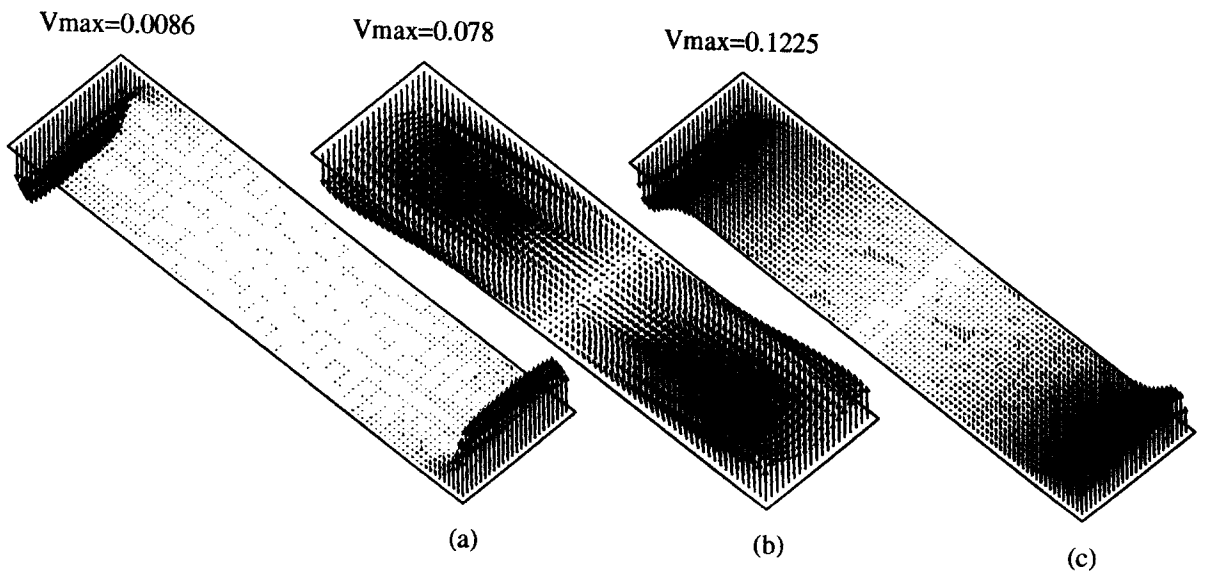

Fig. 7. Velocity vectors in the (Lh)-plane at Gr = 5×10^4 and Ha = 150 for three orientations of the applied magnetic field ((a) B_y case, (b) B_z case, and (c) B_x case).

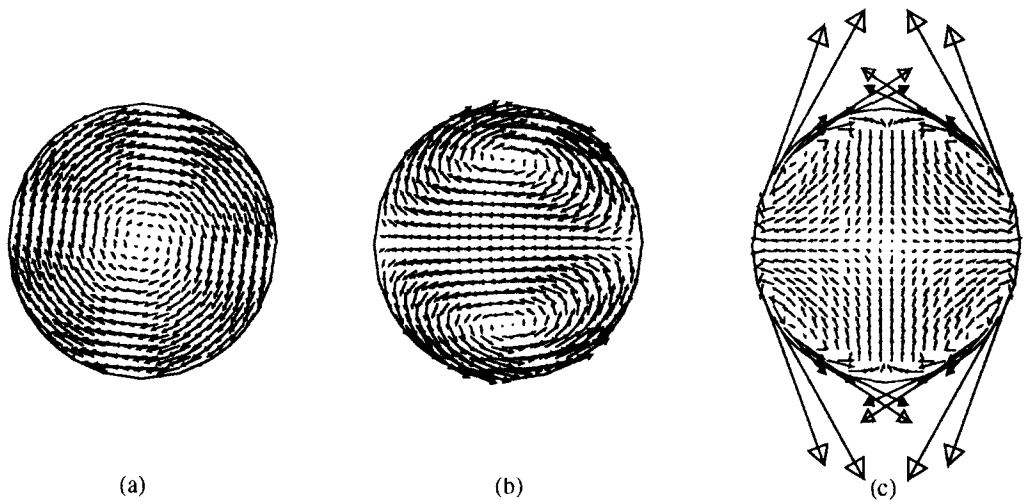

Fig. 8. The electric current projection in a cross-sectional plane ($z = 0.5$) at $Gr = 5 \times 10^4$ and $Ha = 150$ for three orientations of the applied magnetic field ((a) B_y case, (b) B_z case, and (c) B_x case) (view from the right).

tional planes (Fig. 8a). The original directly induced current is horizontal. But, because of the electrically insulating walls, electric potential appears in order to make the current lines closed in the fluid (Fig. 9a). Here, contrary to the parallelepiped case [13], there are no zones where the electric current becomes parallel to $\boldsymbol{B}_0$, which explains the absence of parallel layers with overvelocity peaks. However, the shape of the electric current leads to a stronger decrease in the core than on the circular side walls, which creates the tendency towards two-dimensionality. It can also be noted that in the core, the potential is not uniform (horizontal gradients) and creates a potential contribution to the current, opposed to the directly induced one.

The decrease of the intensity of the flow can be characterized by the evolution with Ha of the maxima of the absolute values of the longitudinal and vertical velocities, values noted respectively W_{max} and V_{max} (Fig. 10). These evolutions reveal an asymptotic behaviour for large Ha values (i.e. $Ha \geq 50$). The maxima are then found to vary as

$$W_{max} \sim Ha^{-2}, \tag{8a}$$

$$V_{max} \sim Ha^{-3/2}. \tag{8b}$$

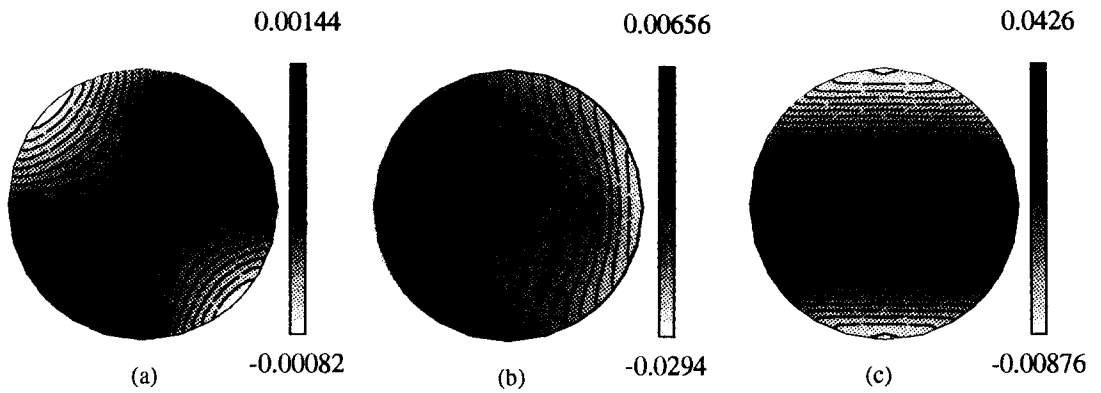

Fig. 9. The electric potential field in a cross-sectional plane ($z = 0.5$) at $Gr = 5 \times 10^4$ and $Ha = 150$ for three orientations of the applied magnetic field ((a) B_y case, (b) B_z case and (c) B_x case) (view from the right).

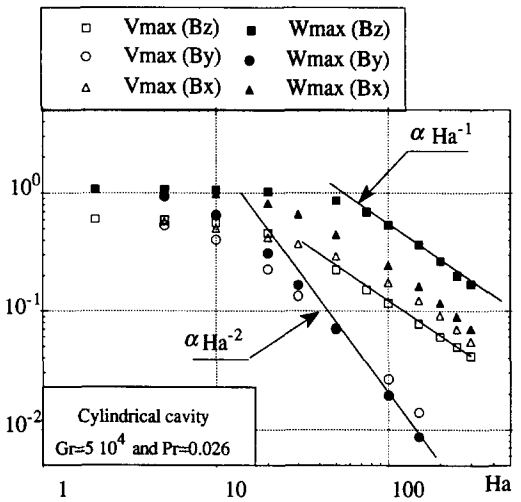

Fig. 10. Plots of the maxima of v and w as a function of Ha at $Gr = 5 \times 10^4$ and $Pr = 0.026$ for three orientations of the magnetic field.

The decrease of W_{max} is in fact smaller than the one given by Eq. (7) because of the potential effect, which is not considered in deriving Eq. (7). This was already shown by asymptotic analysis for large Ha in Ref. [14].

3.3. Longitudinal magnetic field (B_z case)

When the constant magnetic field is applied longitudinally, the main effect is observed on the vertical velocity, which is perpendicular to $\boldsymbol{B}$. A strong decrease is obtained in the core region, whereas the largest velocities appear in two layers (parallel layers) near the circular lateral walls (Fig. 7b). In contrast with the B_y case, the vertical velocities are non-zero over the whole length of the cavity. The horizontal velocity is barely affected by the overvelocities effect in the parallel layers. A further modification (clearly evident for $Ha \geq 200$) corresponds to a weak reverse flow in the core region in a small area around the centre of the circular cross sections (Fig. 11). From the results it can be noted that the length and the width of this reverse flow region increase when Ha is increased.

Concerning the electric current, the directly induced one comes principally from interaction with the vertical velocity component, mainly near the lateral and end walls. Rather than generating long longitudinal current loops, conservation of the current still occurs mainly in cross-sectional planes with the creation of two superposed counter-rotating loops, with opposite senses of rotation in the right and left parts of the cavity (Fig. 8b). This occurs because the electric potential gives the strongest gradients in these cross-sectional planes (Fig. 9b). It can be also noted that the electric quantities have anti-symmetric properties as in the B_y case.

It is clear from the current structure that the currents act directly through the Lorentz force ($\boldsymbol{J} \times \boldsymbol{B}$) to reduce the vertical velocity component, mainly in the centre part of the cross-sectional planes. In the zones near the circular lateral walls the current is no longer horizontal and larger velocities are obtained. In addition, the electric current loops observed in cross-sectional planes, perpendicular to the applied magnetic field, generate concentric electromagnetic forces, which are either convergent or divergent depending on the sense of circulation, and give rise to local overpressures and underpressures, respectively. New longitudinal pressure gradients are then induced, which are responsible for the appearance of the previously observed reverse flows.

The characteristic decrease of the flow with increasing Ha corresponds to Ha^{-1} asymptotic variation for the velocity maxima W_{max} and V_{max} (Fig. 10), which is much smaller than in the B_y case, and it occurs for larger Ha values.

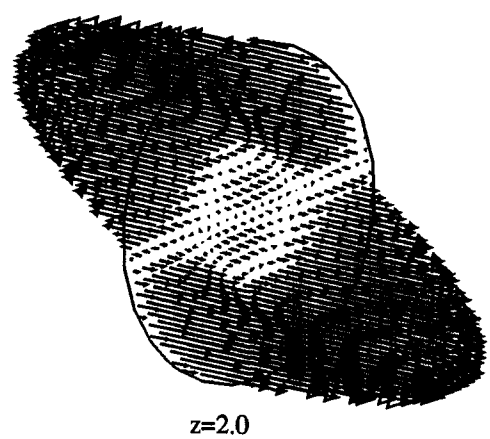

Fig. 11. Velocity vectors in the (Tv)-plane at $Gr = 5 \times 10^4$ and $Ha = 250$ in the B_z case.

3.4. Transverse magnetic field (B_x case)

When the magnetic field is applied along the transverse direction, a decrease of the magnitude of the velocities is first observed followed by a change in the shape of the velocity profiles. The flow becomes two dimensional with only small variations along the transverse direction x except a quick decrease of the velocities near the circular lateral walls where the no-slip condition holds (Figs. 6c and 7c). The horizontal velocity profile along y becomes also linear in the core.

In fact, in two-dimensional cavities, it can be shown that no damping is expected because the induced electric current is zero everywhere [13]. Here, although the electric potential tends to counterbalance the directly induced current (iso-lines of the electric potential in the (Lv)-plane similar to streamlines), the induced electric current in the cavity is no longer zero. The current in the middle zone of the cross-sectional planes goes towards the centre line of the cross section in the upper part and in the opposite sense in the lower part, as would give the directly induced current (Fig. 8c). The potential effect (Fig. 9c) is then not strong enough to balance this direct current. In fact, in the vicinity of the circular lateral boundaries, there is a preponderance of the inverse potential current leading to the creation of four counter-rotative loops in the cross-sectional planes (Fig. 8c). The velocity then goes down faster in the core than along the circular lateral walls, which tends to promote two-dimensional flows. This corresponds in fact to the usual magnetohydrodynamic effect, the tendency towards two-dimensionality for vortices whose axis is parallel to the applied magnetic field [15].

Concerning the horizontal velocity profile along y, it has been shown in Ref. [14] by asymptotic analysis that the expected profile for high Ha is given by

$$w = -\frac{\mathrm{Gr}}{\mathrm{Ha}} y\sqrt{0.25 - y^2}\,. \tag{9}$$

From Eq. (9) it is clear that when Ha becomes large enough a linear variation of the horizontal velocity profile with y will exist around $y = 0$, but it will not affect the whole profile as in the B_y case.

The decrease of the intensity of flow with increasing Ha affects more symmetrically the values of $W_{\max}$ and $V_{\max}$ (Fig. 10). For large Ha (up to Ha = 300), the decrease follows roughly a Ha^{-1} law, in agreement with the asymptotic tendency given by Eq. (9).

4. Conclusion

This study of the effect of a constant magnetic field on three-dimensional buoyancy-induced flows in cylindrical cavities has shown important results. An increase in the strength of the magnetic field causes the flow to evolve both in magnitude and in form. The intensity of the flow is in all cases reduced, with generally an asymptotic variation beyond a certain Ha value, which depends on the direction of the applied constant magnetic field. In our moderate aspect ratio cavity, the decrease of the flow is stronger for the vertical field orientation, and weaker for the two other orientations (Fig. 10). The structural changes lead to the appearance of parallel layers in the longitudinal orientation case. Such layers are characterized by stronger velocities on each side of the central zone with more reduced flow. Different results are obtained for the vertical and transverse field orientation. The main effect is the tendency of the flow towards two-dimensionality with a linear horizontal velocity profile along y. All these structural changes are in fact strongly connected to the induced current distribution inside the cavity, which is specific for each magnetic field orientation.

Acknowledgements

We wish to thank Professor R. Moreau from MADYLAM and Doctor J.P. Garandet from CEN Grenoble for helpful discussions of this work. This work is supported by the "Centre National des Etudes Spatiales" within the frame of the micro-gravity program. The calculations were carried out on a Cray YMP C98 computer with the support of the CNRS through the "Institut du développement et des ressources en informatique scientifique".

References

[1] P. Bontoux, B. Roux, G.H. Schiroky, B.L. Markham and F. Rosenberger, Int. J. Heat Mass Transfer 29 (1986) 227.
[2] P. Bontoux, C. Smutek, B. Roux and J.M. Lacroix, J. Fluid Mech. 169 (1986) 211.
[3] A. Bejan and C.L. Tien, Int. J. Heat Mass Transfer 21 (1978) 701.
[4] R.W. Series and D.T.J. Hurle, J. Crystal Growth 113 (1991) 305.
[5] D.T.J. Hurle, E. Jakeman and C.P. Johnson, J. Fluid Mech. 64 (1974) 565.
[6] J. Baumgartl and G. Müller, in: Proc. VIIIth Eur. Symp. on Materials and Fluid Sciences in Microgravity (ESA SP-333, 1992) (ESA Publ. Division c/o ESTEC, Noordwijk, The Netherlands) p. 161.
[7] J. Baumgartl, A. Hubert and G. Müller, Phys. Fluids A 5 (1993) 3280.
[8] H. Ozoe and K. Okada, Int. J. Heat Mass Transfer 32 (1989) 1939.
[9] L. Davoust, R. Moreau, R. Bolcato, T. Alboussière, A.C. Neubrand and J.P. Garandet, in: Proc. of the 2nd Int. Conf. on Energy Transfer in Magnetohydrodynamic Flows, Aussois, France (1995) p. 15.
[10] G.E. Karniadakis, M. Israeli and S.A. Orszag, J. Comp. Phys. 97 (1991) 414.
[11] K.Z. Korczak and A.T. Patera, J. Comp. Phys. 62 (1986) 361.
[12] J.P. Garandet, T. Alboussière and R. Moreau, Int. J. Heat Mass Transfer 35 (1992) 741.
[13] H. Ben Hadid and D. Henry, J. Fluid Mech., to be published.
[14] T. Alboussière, Thèse de Doctorat de l'Institut National Polytechnique de Grenoble (1994).
[15] R. Moreau, Magnetohydrodynamics, Fluid Mechanics and its Applications Vol. 3 (Kluwer, Dordrecht, 1990).